Received: 16 October 2023 | Revised: 11 March 2024 | Accepted: 25 March 2024

DOI: 10.1002/hipo.23606

RAPID COMMUNICATION

WILEY

Automated protocols for delineating human hippocampal subfields from 3 Tesla and 7 Tesla magnetic resonance imaging data

Alice L. Hickling | Ian A. Clark | Yan I. Wu | Eleanor A. Maguire

Wellcome Centre for Human Neuroimaging, Department of Imaging Neuroscience, UCL Queen Square Institute of Neurology, University College London, London, UK

Correspondence
Eleanor A. Maguire, Wellcome Centre for Human Neuroimaging, Department of Imaging Neuroscience, UCL Queen Square Institute of Neurology, University College London, London, UK.
Email: e.maguire@ucl.ac.uk

Funding information
Wellcome trust, Grant/Award Numbers: 101759/Z/13/Z, 210567/Z/18/Z, 203147/Z/16/Z

Abstract

Researchers who study the human hippocampus are naturally interested in how its subfields function. However, many researchers are precluded from examining subfields because their manual delineation from magnetic resonance imaging (MRI) scans (still the gold standard approach) is time consuming and requires significant expertise. To help ameliorate this issue, we present here two protocols, one for 3T MRI and the other for 7T MRI, that permit automated hippocampus segmentation into six subregions, namely dentate gyrus/cornu ammonis (CA)4, CA2/3, CA1, subiculum, pre/parasubiculum, and uncus along the entire length of the hippocampus. These protocols are particularly notable relative to existing resources in that they were trained and tested using large numbers of healthy young adults (n = 140 at 3T, n = 40 at 7T) whose hippocampi were manually segmented by experts from MRI scans. Using inter-rater reliability analyses, we showed that the quality of automated segmentations produced by these protocols was high and comparable to expert manual segmenters. We provide full open access to the automated protocols, and anticipate they will save hippocampus researchers a significant amount of time. They could also help to catalyze subfield research, which is essential for gaining a full understanding of how the hippocampus functions.

KEYWORDS
3 Tesla, 7 Tesla, automated segmentation, hippocampus subfields, structural MRI

The hippocampus is composed of distinct subfields that have different functions (Bonnici et al., 2013; Neunuebel & Knierim, 2014; Zeidman et al., 2015) and connectivity patterns (Dalton et al., 2019, 2022). Studying human hippocampal subfields typically requires them to be delineated from structural magnetic resonance imaging (MRI) scans. Manual segmentation of subfields from such scans remains the gold standard approach (Dalton et al., 2017; Wisse et al., 2017). However, there are currently numerous protocols available that differ on a range of parameters. These include the location of borders between subfields, the granularity with which specific subfields can be individually delineated, and whether nor not the full length of the hippocampus is segmented. Automated methods for subfield segmentation have also been developed (e.g., Augustinack et al., 2013; Fischl et al., 2009; Hadar et al., 2018; Iglesias et al., 2015; Pipitone et al., 2014; Van Leemput et al., 2009; Wisse et al., 2016; Yushkevich et al., 2010, 2015a) which essentially recapitulate these protocol differences. This variety of approaches hinders the ability to integrate and interpret findings across studies.

To address this issue, the Hippocampal Subfield Group (HSG: http://www.hippocampalsubfields.com) was convened. It includes colleagues from around the world who are working toward the

production of a reliable, validated, harmonized protocol for manual segmentation of hippocampal subfields and associated medial temporal lobe regions. This huge undertaking is progressing (Olsen et al., 2019; Wisse et al., 2017; Yushkevich et al., 2015b), and will eventually be an invaluable and unifying resource for the field of hippocampus neuroscience.

In the meantime, we previously devised a detailed manual subfield segmentation protocol that is faithful to our current understanding of hippocampal anatomy (Dalton et al., 2017). We favor this protocol because it allows the whole hippocampus to be segmented into six subregions: dentate gyrus (DG)/Cornu Ammonis (CA)4, CA2/3, CA1, subiculum, a combined area comprising the presubiculum and parasubiculum hereafter called the pre/parasubiculum, and the uncus. It takes approximately 8 h for an expert to segment a person's two hippocampi from T2-weighted isotropic voxel MRI scans using this protocol. But such expertise is not available in all research groups, and even when it is, the time sink involved often prohibits conducting experiments at scale, such as those examining individual differences.

Consequently, the goal of the current study was to devise an automated subfield segmentation protocol based on the Dalton et al. (2017) approach. We could pursue this aim thanks to two open access resources. The first is the recently released open access dataset from Clark and Maguire (2023) that includes the largest set of manually segmented hippocampal subfields of healthy young adults that is currently available. The second is the software package Automatic Segmentation of Hippocampal Subfields (ASHS; Yushkevich et al., 2015a) which is free, open source and editable. ASHS can be retrained using one's own MRI data and segmentation protocol to produce an ASHS "atlas package" that can then be used to automatically segment subfields from new MRI scans.

The 3 Tesla (3T) MRI data from Clark and Maguire (2023) that we used to build an atlas were from the manually segmented hippocampal subfields of 140 healthy adult participants (81 females) aged between 20 and 41 years old (mean age = 29.09, SD = 5.61). We complemented this 3T endeavor with newly-segmented data from 40 (different) healthy adult participants (26 females) aged between 18 and 33 years old (mean age = 23.8, SD = 3.99) who were scanned at 7 Tesla (7T). We therefore aimed to produce two atlases, one for 3T MRI data and another for 7T MRI data. People with hobbies or vocations known to be associated with the hippocampus (e.g. licensed London taxi drivers) were excluded. Participants were reimbursed £10 per hour for taking part. All participants gave written informed consent, and the study was conducted in accordance with the approval of the University College London Research Ethics Committee (project IDs: 6743/001 and 18721/001).

For the n = 140 3T MRI data, we randomly allocated 125 of the participants to a 3T training group which was used to build the 3T ASHS atlas package. This provided an unprecedented opportunity for the ASHS algorithm to train on a large number of expertly segmented hippocampi. The remaining 15 participants were assigned to a 3T testing group that was used to assess the quality of automatic segmentations produced by the 3T ASHS atlas package. For the n = 40 7T MRI data, we randomly allocated 30 participants to a 7T training group which was used for training the 7T ASHS atlas package, and the remaining 10 participants to a 7T testing group that was used to assess the 7T ASHS atlas package.

The 3T data were collected using a Siemens Magnetom TIM Trio 3T MRI system with a 32 channel head coil. T2-weighted partial volume images were acquired (voxel size = 0.52 × 0.52 × 0.50 mm) using a 3D turbo spin echo sequence. Full details of the sequence are available in previous publications (Clark et al., 2023; Clark & Maguire, 2023; Dalton et al., 2017, 2019). Of note, scans with isotropic voxels, such as those here, have equivalent resolution in all orientations, which is particularly important for convoluted structures like the hippocampus, which can contain undulations in the subfields. For each participant, three images were acquired (each taking 13 m) and up to three high quality images were coregistered, denoised and averaged. This averaging and denoising method improved the signal-to-noise ratio of the T2-weighted image used for hippocampal subfield segmentation. ASHS also requires a T1-weighted image for initial localization of the whole hippocampus. For this we used whole brain T1-weighted gradient echo images with an isotropic resolution of 800 μm that were acquired as part of a Multi-Parameter Mapping quantitative imaging protocol (taking 25 m in total; Callaghan et al., 2015; Callaghan et al., 2019). Full details of this sequence can be found in Clark et al. (2020), Clark et al. (2021), Clark et al. (2022) and Clark and Maguire (2023).

The 7T MRI data were acquired on a Siemens Magnetom Terra 7T MRI system with an 8 channel head coil for localized transmission, operating in a quadrature-like ("TrueForm") mode, with a 32-channel head coil insert for reception. The partial volume T2-weighted 3T MRI sequence was adapted for 7T MRI to yield the voxel size 0.52 × 0.52 × 0.50 mm, TR = 3500 ms, echo time (TE) = 229 ms, flip angle = 8°, field of view = 200 × 169 mm x 56 mm, matrix = 384 × 324 × 112, partitions = 112, partition thickness = 0.5 mm, partition oversampling = 14.3%, GRAPPA × 2 in phase-encoding (PE) direction, bandwidth = 868 Hz/Px, echo spacing = 3.83 ms, turbo factor = 176, echo train duration = 548 ms, averages = 1.4. For each participant, two images were acquired (each taking 10 m and 25 s) and up to two high quality images were coregistered, denoised, and averaged prior to being used for segmentation of the hippocampal subfields. Of note, such was the image quality at 7T that often one image would have been sufficient for subfield segmentation, which could mean shorter acquisition times for future studies. Whole brain T1-weighted images with an isotropic resolution of 650 μm were also acquired using a Magnetization Prepared 2 Rapid Acquisition Gradient Echo (MP2RAGE) sequence (Marques et al., 2010), taking 8 m 42 s, with TR = 5000 ms, TE = 2.54 ms, TI = 900 ms, and 2750 ms, 5° and 3° flip angles, field of view = 208 × 208 × 156 mm^3, and GRAPPA × 3 in PE direction.

ITK Snap software version 3.2.0 was used to manually delineate the hippocampal subfields on the averaged and denoised T2-weighted images in line with the Dalton et al. (2017) protocol. For each participant the two hippocampi were manually segmented into six subregions: DG/CA4, CA2/3, CA1, subiculum, pre/parasubiculum, and uncus.

We first used inter-rater reliability analysis to assess the manual hippocampal segmentations. A second researcher independently

segmented the hippocampi of 20 out of the 125 participants in the 3T training group, and 9 out of the 30 participants in the 7T training group. The Dice similarity coefficient (Dice, 1945), which ranges from 0 (no overlap) to 1 (complete overlap), was used to calculate the degree of overlap between the subfield masks produced by the first and second researchers. The results are shown on Table 1, and for both 3T and 7T MRI they were comparable to previous studies using this protocol (e.g., Barry et al., 2021; Clark et al., 2023; Dalton et al., 2019) and other approaches (e.g., Berron et al., 2017; Bonnici et al., 2013; Chadwick et al., 2014; Lee et al., 2014; Palombo et al., 2013; Yeung et al., 2019).

Having established that the manual segmentations were reliable, we next created the ASHS atlases. We trained ASHS on the manual hippocampal subfield segmentations of the 3T training group sample (125 participants) and separately on the 7T training group sample (30 participants). Several ASHS configuration parameters were adjusted to optimize the software for the $0.52 \times 0.52 \times 0.50$ mm voxel size of our T2-weighted images. The ASHS training process works by first applying deformable coregistration of the T1-weighted image, T2-weighted image and hippocampal subfield masks to an unbiased population template. Automatic segmentations are then produced by deformably coregistering the T2-weighted image of each participant to that of all other participants, and applying joint label fusion (Wang et al., 2013). Finally, corrective learning classifiers (Wang et al., 2011) are trained by comparing the automatic segmentations with the manual segmentation of the same T2-weighted image; see Yushkevich, Pluta, et al. (2015) for full details of the ASHS pipeline. We used leave-one-out cross-validation to train the 7T ASHS atlas package and, due to the larger 3T training group sample and for computational efficiency, we used leave-five-out cross-validation to train the 3T ASHS atlas package (see Supporting Information Table S1 for results based on the cross-validation tests).

We then used our 3T and 7T ASHS atlas packages to segment the hippocampi of participants in the new 3T test group (15 participants) and new 7T test group (10 participants) respectively. When used to segment new hippocampi, ASHS produces automatic segmentations in the same way as it does during training. Then it uses the trained corrective learning classifiers to correct the automatic segmentation. We evaluated performance of the 3T and 7T ASHS atlas packages by using inter-rater reliability analysis to compare the automatic segmentations with corresponding manual segmentations of the same test samples. The results are shown on Table 2. As is evident for both 3T and 7T atlases, Dice similarity coefficients were comparable to, if not better than (see Figure 1), previous studies involving expert manual segmenters using this protocol (e.g., Barry et al., 2021; Clark et al., 2023; Dalton et al., 2019) and other approaches (e.g., Berron et al., 2017; Bonnici et al., 2013; Chadwick et al., 2014; Lee et al., 2014; Palombo et al., 2013; Yeung et al., 2019).

TABLE 1 Inter-rater reliability results for the two manual segmenters.

	Dice similarity coefficient (mean ± SD)			
	3T MRI		7T MRI	
Subfield	Left	Right	Left	Right
Dentate gyrus	0.84 ± 0.02	0.85 ± 0.03	0.87 ± 0.02	0.86 ± 0.03
CA2/3	0.67 ± 0.04	0.68 ± 0.04	0.69 ± 0.02	0.68 ± 0.04
CA1	0.78 ± 0.03	0.79 ± 0.02	0.78 ± 0.03	0.80 ± 0.02
Subiculum	0.81 ± 0.02	0.79 ± 0.02	0.81 ± 0.03	0.79 ± 0.03
Pre/parasubiculum	0.71 ± 0.03	0.69 ± 0.03	0.70 ± 0.04	0.72 ± 0.02
Uncus	0.82 ± 0.03	0.84 ± 0.02	0.88 ± 0.03	0.86 ± 0.04

Note: Two researchers independently segmented the hippocampi of 20 out of the 125 participants in the 3T training group, and 9 out of the 30 participants in the 7T training group.

TABLE 2 Reliability results for the Automatic Segmentation of Hippocampal Subfields (ASHS) atlases when compared to an independent set of manually segmented images.

	Dice similarity coefficient (mean ± SD)			
	3T MRI ASHS atlas		7T MRI ASHS atlas	
Subfield	Left	Right	Left	Right
Dentate gyrus	0.88 ± 0.03	0.89 ± 0.01	0.87 ± 0.03	0.89 ± 0.01
CA2/3	0.74 ± 0.04	0.75 ± 0.05	0.75 ± 0.05	0.78 ± 0.03
CA1	0.81 ± 0.03	0.83 ± 0.02	0.81 ± 0.03	0.82 ± 0.02
Subiculum	0.83 ± 0.02	0.82 ± 0.02	0.83 ± 0.02	0.84 ± 0.02
Pre/parasubiculum	0.72 ± 0.05	0.72 ± 0.05	0.71 ± 0.05	0.74 ± 0.02
Uncus	0.85 ± 0.02	0.85 ± 0.02	0.84 ± 0.03	0.86 ± 0.03

Note: Our 3T and 7T ASHS atlas packages were used to segment the hippocampi of participants in a new 3T test group ($n = 15$) and a new 7T test group ($n = 10$), respectively.

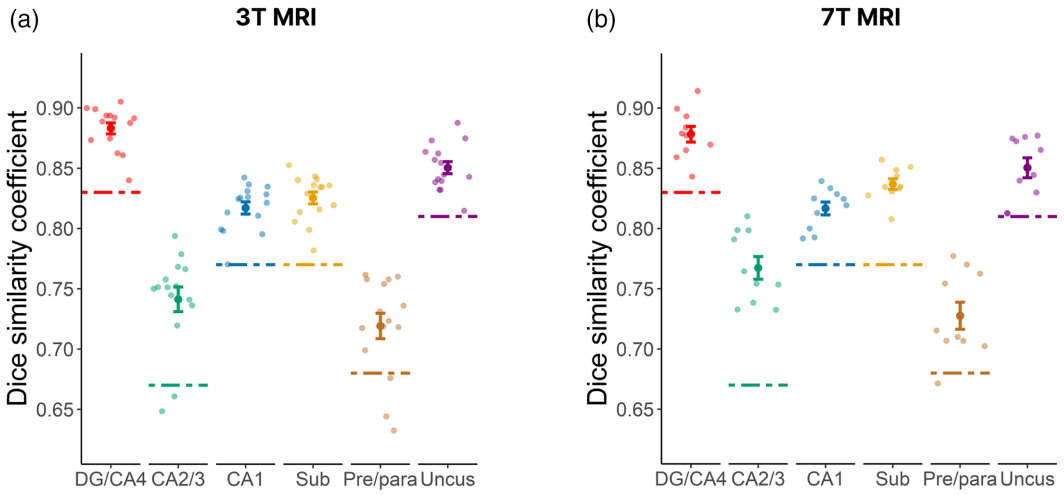

FIGURE 1 Dice similarity coefficients for the comparison between Automatic Segmentation of Hippocampal Subfields (ASHS) automatic segmentations and the corresponding manual segmentations, where (a) relates to our 3T ASHS atlas package used to segment hippocampi from new 3T MRI data (n = 15) and (b) relates to our 7T ASHS atlas package used to segment hippocampi from new 7T MRI data (n = 10). The overall mean Dice similarity coefficients are plotted with opaque points and the mean Dice similarity coefficients for each test participant's data are plotted with transparent points. Error bars indicate the standard error of the mean. To aid interpretation, the dashed lines provide an approximate indication of the typical inter-rater reliability thresholds between human manual segmenters for the protocol used here. DG, dentate gyrus; Sub, subiculum; Pre/para, pre/parasubiculum.

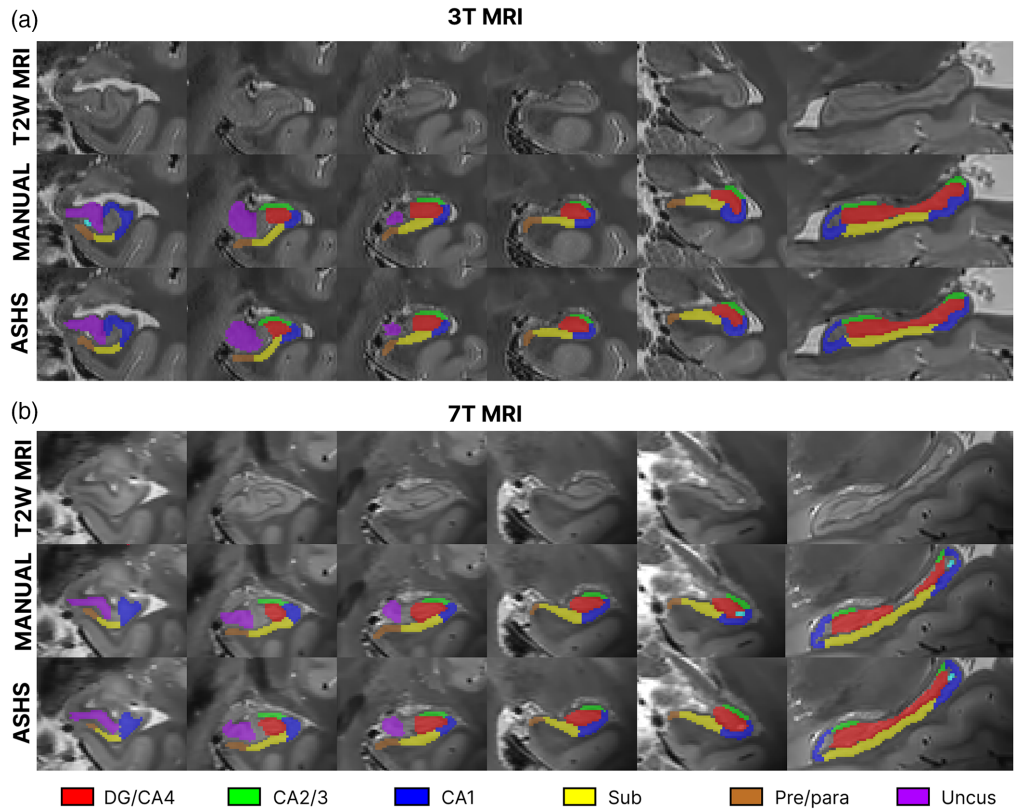

FIGURE 2 Example segmentations, one from a 3T MRI participant (upper panels) and one from a 7T MRI participant (lower panels), performed using (a) the 3T ASHS atlas package to segment hippocampi from new 3T MRI data and (b) the 7T ASHS atlas package to segment hippocampi from new 7T MRI data. In both (a) and (b), the top row displays the raw T2-weighted image, the second row shows a manual segmentation of the hippocampal subfields and the bottom row displays the ASHS automatic segmentation. Note that light blue areas are cysts. T2W, T2-weighted; DG, dentate gyrus; Sub, subiculum; Pre/para, pre/parasubiculum. The images shown for 3T and 7T are from approximately similar locations along the length of the hippocampus. See Supporting Information Figure S1 for further examples.

When visually inspecting automatic segmentations and their corresponding manual segmentations, the subregion masks appeared very similar (see Figure 2; for further examples see Supporting Information Figure S1). There were some minor local differences, which are also common in manual segmentations performed by different human segmenters. These two ASHS atlas packages can, therefore, be used to automatically segment subfields from new 3T and 7T T2-weighted structural MRI data with isotropic voxels. The atlases, along with a README file containing information about the IT requirements and a step-by-step guide for using the atlases, are available on Figshare (https://doi.org/10.6084/m9.figshare.24298891).

There are several caveats that should be borne in mind in relation to these ASHS atlases. They were built using the MRI scans of healthy young adults, and so would be best used to segment subfields in scans from similar people. As many participants in cognitive neuroscience experiments are from the age groups scanned here, we hope the atlases will be useful. ASHS also requires T2-weighted scans, and indeed such scans are, in our experience, best suited to delineating the hippocampal subfields. We also strongly advocate having scans with isotropic voxels particularly for an undulating structure like the hippocampus. Atlas users should therefore acquire data with isotropic voxels in order to achieve maximum benefit. A final point to note is that our atlases focus solely on the hippocampus. For researchers interested in adjacent cortical areas such as the entorhinal or perirhinal cortices, the large open access Clark and Maguire (2023) dataset and the editable ASHS software provide the opportunity to segment and build new atlases that include these regions in the future.

In summary, here we demonstrated that the whole hippocampus can be automatically segmented from 3T and 7T MRI scans with isotropic voxels into six subregions according to a detailed subfield segmentation protocol. We provide free, open access to the ASHS atlas packages we developed and that makes this possible. We showed that the quality of automated segmentations produced by these ASHS atlas packages is high when assessed by inter-rater reliability analyses, which is the method typically used for checking the quality of manual segmentations. We anticipate that these atlases will save researchers a significant amount of time, especially when conducting subfield experiments at scale. Moreover, we hope that the ability to automatically segment subfields will allow more research groups to conduct subfield experiments, which will be essential for gaining a full understanding of how the hippocampus functions.

ACKNOWLEDGMENTS

Thanks to Anna Monk, Victoria Hotchin, Gloria Pizzamiglio, and Alice Liefgreen for assistance with 3T MRI data collection, Marshall Dalton for advice about hippocampal subfield anatomy, Nikolaus Weiskopf for his work on the 3T T2-weighted MRI sequence, and David Thomas for adapting this sequence for 7T MRI. We are also grateful to members of the Penn Image Computing and Science Laboratory, Department of Radiology, University of Pennsylvania for developing the ASHS software and for making it free, open access, and editable.

FUNDING INFORMATION

This research was supported by a Wellcome Principal Research Fellowship to E.A.M. (101759/Z/13/Z; 210567/Z/18/Z) and a Wellcome Centre Award to the Wellcome Centre for Human Neuroimaging (203147/Z/16/Z).

CONFLICT OF INTEREST STATEMENT

The authors declare no competing interests.

DATA AVAILABILITY STATEMENT

Our 3T and 7T ASHS atlas packages are fully open access and are available here: https://doi.org/10.6084/m9.figshare.24298891.

ORCID

Alice L. Hickling https://orcid.org/0000-0001-8147-5996
Eleanor A. Maguire https://orcid.org/0000-0002-9470-6324

REFERENCES

Augustinack, J. C., Huber, K. E., Stevens, A. A., Roy, M., Frosch, M. P., van der Kouwe, A. J., Wald, L. L., Van Leemput, K., McKee, A. C., Fischl, B., & Alzheimer's Disease Neuroimaging Initiative. (2013). Predicting the location of human perirhinal cortex, Brodmann's area 35, from MRI. *NeuroImage*, *64*, 32–42. https://doi.org/10.1016/j.neuroimage.2012.08.071

Barry, D. N., Clark, I. A., & Maguire, E. A. (2021). The relationship between hippocampal subfield volumes and autobiographical memory persistence. *Hippocampus*, *31*(4), 362–374. https://doi.org/10.1002/hipo.23293

Berron, D., Vieweg, P., Hochkeppler, A., Pluta, J. B., Ding, S. L., Maass, A., Luther, A., Xie, L., Das, S. R., Wolk, D. A., Wolbers, T., Yushkevich, P. A., Düzel, E., & Wisse, L. E. M. (2017). A protocol for manual segmentation of medial temporal lobe subregions in 7 tesla MRI. *NeuroImage Clinical*, *15*, 466–482. https://doi.org/10.1016/j.nicl.2017.05.022

Bonnici, H. M., Chadwick, M. J., & Maguire, E. A. (2013). Representations of recent and remote autobiographical memories in hippocampal subfields. *Hippocampus*, *23*(10), 849–854. https://doi.org/10.1002/hipo.22155

Callaghan, M. F., Josephs, O., Herbst, M., Zaitsev, M., Todd, N., & Weiskopf, N. (2015). An evaluation of prospective motion correction (PMC) for high resolution quantitative MRI. *Frontiers in Neuroscience*, *9*, 97. https://doi.org/10.3389/fnins.2015.00097

Callaghan, M. F., Lutti, A., Ashburner, J., Balteau, E., Corbin, N., Draganski, B., Helms, G., Kherif, F., Leutritz, T., Mohammadi, S., Phillips, C., Reimer, E., Ruthotto, L., Seif, M., Tabelow, K., Ziegler, G., & Weiskopf, N. (2019). Example dataset for the hMRI toolbox. *Data in Brief*, *25*, 104132. https://doi.org/10.1016/j.dib.2019.104132

Chadwick, M. J., Bonnici, H. M., & Maguire, E. A. (2014). CA3 size predicts the precision of memory recall. *Proceedings of the National Academy of Sciences of the United States of America*, *111*(29), 10720–10725. https://doi.org/10.1073/pnas.1319641111

Clark, I. A., Callaghan, M. F., Weiskopf, N., & Maguire, E. A. (2021). The relationship between hippocampal-dependent task performance and hippocampal grey matter myelination and iron content. *Brain and Neuroscience Advances*, *5*, 23982128211011923. https://doi.org/10.1177/23982128211011923

Clark, I. A., Dalton, M. A., & Maguire, E. A. (2023). Posterior hippocampal CA2/3 volume is associated with autobiographical memory recall ability in lower performing individuals. *Scientific Reports*, *13*, 7924. https://doi.org/10.1038/s41598-023-35127-2

Clark, I. A., & Maguire, E. A. (2023). Release of cognitive and multimodal MRI data including real-world tasks and hippocampal subfield segmentations. *Scientific Data*, *10*(1), 540. https://doi.org/10.1038/s41597-023-02449-9

Clark, I. A., Mohammadi, S., Callaghan, M. F., & Maguire, E. A. (2022). Conduction velocity along a key white matter tract is associated with autobiographical memory recall ability. *eLife*, *11*, e79303. https://doi.org/10.7554/eLife.79303

Clark, I. A., Monk, A. M., Hotchin, V., Pizzamiglio, G., Liefgreen, A., Callaghan, M. F., & Maguire, E. A. (2020). Does hippocampal volume explain performance differences on hippocampal-dependant tasks? *NeuroImage*, *221*, 117211. https://doi.org/10.1016/j.neuroimage.2020.117211

Dalton, M. A., D'Souza, A., Lv, J., & Calamante, F. (2022). New insights into anatomical connectivity along the anterior-posterior axis of the human hippocampus using in vivo quantitative fibre tracking. *eLife*, *11*, e76143. https://doi.org/10.7554/eLife.76143

Dalton, M. A., McCormick, C., & Maguire, E. A. (2019). Differences in functional connectivity along the anterior-posterior axis of human hippocampal subfields. *NeuroImage*, *192*, 38–51. https://doi.org/10.1016/j.neuroimage.2019.02.066

Dalton, M. A., Zeidman, P., Barry, D. N., Williams, E., & Maguire, E. A. (2017). Segmenting subregions of the human hippocampus on structural magnetic resonance image scans: An illustrated tutorial. *Brain and Neuroscience Advances*, *1*, 2398212817701448. https://doi.org/10.1177/2398212817701448

Dice, L. R. (1945). Measures of the amount of ecologic association between species. *Ecology*, *26*, 297–302.

Fischl, B., Stevens, A. A., Rajendran, N., Yeo, B. T., Greve, D. N., Van Leemput, K., Polimeni, J. R., Kakunoori, S., Buckner, R. L., Pacheco, J., Salat, D. H., Melcher, J., Frosch, M. P., Hyman, B. T., Grant, P. E., Rosen, B. R., van der Kouwe, A. J., Wiggins, G. C., Wald, L. L., & Augustinack, J. C. (2009). Predicting the location of entorhinal cortex from MRI. *NeuroImage*, *47*(1), 8–17. https://doi.org/10.1016/j.neuroimage.2009.04.033

Hadar, P. N., Kini, L. G., Coto, C., Piskin, V., Callans, L. E., Chen, S. H., Stein, J. M., Das, S. R., Yushkevich, P. A., & Davis, K. A. (2018). Clinical validation of automated hippocampal segmentation in temporal lobe epilepsy. *NeuroImage Clinical*, *20*, 1139–1147. https://doi.org/10.1016/j.nicl.2018.09.032

Iglesias, J. E., Augustinack, J. C., Nguyen, K., Player, C. M., Player, A., Wright, M., Roy, N., Frosch, M. P., McKee, A. C., Wald, L. L., Fischl, B., Van Leemput, K., & Alzheimer's Disease Neuroimaging Initiative. (2015). A computational atlas of the hippocampal formation using ex vivo, ultra-high resolution MRI: Application to adaptive segmentation of in vivo MRI. *NeuroImage*, *115*, 117–137. https://doi.org/10.1016/j.neuroimage.2015.04.042

Lee, J. K., Ekstrom, A. D., & Ghetti, S. (2014). Volume of hippocampal subfields and episodic memory in childhood and adolescence. *NeuroImage*, *94*, 162–171. https://doi.org/10.1016/j.neuroimage.2014.03.019

Marques, J. P., Kober, T., Krueger, G., van der Zwaag, W., Van de Moortele, P. F., & Gruetter, R. (2010). MP2RAGE, a self bias-field corrected sequence for improved segmentation and T1-mapping at high field. *NeuroImage*, *49*(2), 1271–1281. https://doi.org/10.1016/j.neuroimage.2009.10.002

Neunuebel, J. P., & Knierim, J. J. (2014). CA3 retrieves coherent representations from degraded input: Direct evidence for CA3 pattern completion and dentate gyrus pattern separation. *Neuron*, *81*(2), 416–427. https://doi.org/10.1016/j.neuron.2013.11.017

Olsen, R. K., Carr, V. A., Daugherty, A. M., la Joie, R., Amaral, R. S. C., Amunts, K., Augustinack, J. C., Bakker, A., Bender, A. R., Berron, D., Boccardi, M., Bocchetta, M., Burggren, A. C., Chakravarty, M. M., Chételat, G., De Flores, R., DeKraker, J., Ding, S. L., Geerlings, M. I., … Hippocampal Subfields Group. (2019). Progress update from the hippocampal subfields group. *Alzheimer's & Dementia: Diagnosis, Assessment & Disease Monitoring*, *11*, 439–449. https://doi.org/10.1016/j.dadm.2019.04.001

Palombo, D. J., Amaral, R. S., Olsen, R. K., Müller, D. J., Todd, R. M., Anderson, A. K., & Levine, B. (2013). KIBRA polymorphism is associated with individual differences in hippocampal subregions: Evidence from anatomical segmentation using high-resolution MRI. *Journal of Neuroscience*, *33*(32), 13088–13093. https://doi.org/10.1523/JNEUROSCI.1406-13.2013

Pipitone, J., Park, M. T., Winterburn, J., Lett, T. A., Lerch, J. P., Pruessner, J. C., Lepage, M., Voineskos, A. N., Chakravarty, M. M., & Alzheimer's Disease Neuroimaging Initiative. (2014). Multi-atlas segmentation of the whole hippocampus and subfields using multiple automatically generated templates. *NeuroImage*, *101*, 494–512. https://doi.org/10.1016/j.neuroimage.2014.04.054

Van Leemput, K., Bakkour, A., Benner, T., Wiggins, G., Wald, L. L., Augustinack, J., Dickerson, B. C., Golland, P., & Fischl, B. (2009). Automated segmentation of hippocampal subfields from ultra-high resolution in vivo MRI. *Hippocampus*, *19*(6), 549–557. https://doi.org/10.1002/hipo.20615

Wang, H., Das, S. R., Suh, J. W., Altinay, M., Pluta, J., Craige, C., Avants, B., Yushkevich, P. A., & Alzheimer's Disease Neuroimaging Initiative. (2011). A learning-based wrapper method to correct systematic errors in automatic image segmentation: Consistently improved performance in hippocampus, cortex and brain segmentation. *NeuroImage*, *55*(3), 968–985. https://doi.org/10.1016/j.neuroimage.2011.01.006

Wang, H., Suh, J. W., Das, S. R., Pluta, J. B., Craige, C., & Yushkevich, P. A. (2013). Multi-atlas segmentation with joint label fusion. *IEEE Transactions on Pattern Analysis and Machine Intelligence*, *35*(3), 611–623. https://doi.org/10.1109/TPAMI.2012.143

Wisse, L. E., Kuijf, H. J., Honingh, A. M., Wang, H., Pluta, J. B., Das, S. R., Wolk, D. A., Zwanenburg, J. J., Yushkevich, P. A., & Geerlings, M. I. (2016). Automated hippocampal subfield segmentation at 7T MRI. *AJNR. American Journal of Neuroradiology*, *37*(6), 1050–1057. https://doi.org/10.3174/ajnr.A4659

Wisse, L. E. M., Daugherty, A. M., Olsen, R. K., Berron, D., Carr, V. A., Stark, C. E. L., Amaral, R. S. C., Amunts, K., Augustinack, J. C., Bender, A. R., Bernstein, J. D., Boccardi, M., Bocchetta, M., Burggren, A., Chakravarty, M. M., Chupin, M., Ekstrom, A., De Flores, R., Insausti, R., … Hippocampal Subfields Group. (2017). A harmonized segmentation protocol for hippocampal and parahippocampal subregions: Why do we need one and what are the key goals? *Hippocampus*, *27*(1), 3–11. https://doi.org/10.1002/hipo.22671

Yeung, L. K., Olsen, R. K., Hong, B., Mihajlovic, V., D'Angelo, M. C., Kacollja, A., Ryan, J. D., & Barense, M. D. (2019). Object-in-place memory predicted by anterolateral entorhinal cortex and parahippocampal cortex volume in older adults. *Journal of Cognitive Neuroscience*, *31*(5), 711–729. https://doi.org/10.1162/jocn_a_01385

Yushkevich, P. A., Amaral, R. S. C., Augustinack, J. C., Bender, A. R., Bernstein, J. D., et al. (2015). Quantitative comparison of 21 protocols for labeling hippocampal subfields and parahippocampal cortical subregions in in vivo MRI: Initial steps towards a harmonized segmentation protocol. *NeuroImage*, *111*, 526–541. https://doi.org/10.1016/j.neuroimage.2015.01.004

Yushkevich, P. A., Pluta, J. B., Wang, H., Xie, L., Ding, S. L., Gertje, E. C., Mancuso, L., Kliot, D., Das, S. R., & Wolk, D. A. (2015). Automated volumetry and regional thickness analysis of hippocampal subfields and medial temporal cortical structures in mild cognitive impairment. *Human Brain Mapping*, *36*(1), 258–287. https://doi.org/10.1002/hbm.22627

Yushkevich, P. A., Wang, H., Pluta, J., Das, S. R., Craige, C., Avants, B. B., Weiner, M. W., & Mueller, S. (2010). Nearly automatic segmentation of hippocampal subfields in in vivo focal T2-weighted MRI. *NeuroImage*, *53*(4), 1208–1224. https://doi.org/10.1016/j.neuroimage.2010.06.040

Zeidman, P., Lutti, A., & Maguire, E. A. (2015). Investigating the functions of subregions within anterior hippocampus. *Cortex*, *73*, 240–256. https://doi.org/10.1016/j.cortex.2015.09.002

SUPPORTING INFORMATION

Additional supporting information can be found online in the Supporting Information section at the end of this article.

How to cite this article: Hickling, A. L., Clark, I. A., Wu, Y. I., & Maguire, E. A. (2024). Automated protocols for delineating human hippocampal subfields from 3 Tesla and 7 Tesla magnetic resonance imaging data. *Hippocampus*, 1–7. https://doi.org/10.1002/hipo.23606